ABSTRACT

MCCALL, JAMES VAUGHN. Performance of a Powered Ankle Exoskeleton Using Neuromuscular Model-Based Control over a Range of Walking Speeds. (Under the direction of Derek G. Kamper).

Powered exoskeletons can improve locomotion performance by providing assistive torques to augment biological moments generated by lower-limb joints [1], [2]. Many exoskeleton controllers are either dependent on *a priori* tuning of parameters based on a restricted set of controlled locomotor tasks (e.g., level treadmill walking at fixed speed) or do not quickly adapt to changing user needs [3], [4]. The effectiveness of these controllers are, therefore, limited to a small subset of functional conditions. Exoskeleton controllers need the capability to automatically adapt to the user's needs to be useful in the real-world.

Past studies have investigated the performance of a neuromuscular model (NMM) controller for a unilateral powered ankle prosthesis on a variety of ground slope conditions and walking speeds [5], [6], and for control of ankle or knee and hip exoskeletons across a range of walking speeds [7], [8]. NMM controllers mimic estimated biological torque according to the joint angle (from which muscle tendon length, contractile element contraction velocity, etc. are calculated). The NMM-controlled prosthesis was able to adjust net work according to walking speed or ground slope; and the NMM-controlled exoskeletons were able to adjust torque according to walking speed.

This study expanded on past work by applying an NMM-controller to bilateral ankle exoskeletons and evaluating performance over a range of high walking speeds. Eight healthy adult participants performed level treadmill walking trials across a range of speeds (1.25 ms^{-1}, 1.50 ms^{-1}, 1.75 ms^{-1}) while either not wearing the exoskeletons, while wearing

the exoskeletons without powered assistance, or while wearing the exoskeletons with powered assistance (total of nine trials per subject). Joint mechanics, metabolic energy consumption, electromyography (EMG) signals (tibialis anterior, soleus, and gastrocnemius), and exoskeleton torque (when applicable) were measured for each trial.

There were no significant changes in metabolic energy consumption due to exoskeletal assistance at any walking speed, despite decreases of biological ankle torque and work in the powered exoskeleton condition. The NMM-controller decreased biological ankle torque and work in the powered condition; exoskeleton work performed did not change significantly across walking speeds. Exoskeleton torque decreased as walking speed increased.

As walking speed increased, stride time decreased. Reduced stride time caused a decrease in virtual muscle activation due to activation dynamics, as the activation level attained is dependent upon the time given to reach the desired level. Decreased stride time decreased the available time for muscle activation, thereby causing decreased activation. Reduced activation caused the virtual muscle tendon unit (vMTU) to produce smaller forces, which further reduced virtual muscle activation at high walking speeds. Additionally, walking in the powered exoskeleton caused increased plantarflexion throughout the stride, which caused the controller to calculate reduced virtual tendon stretch, and therefore reduced virtual MTU force. These factors resulted in the controller being unable to increase torque with walking speed. NMM-based walking simulations, which are successful at achieving high walking speeds, incorporate a feedforward component to keep muscle activation high [9], [10]. Proportional myoelectric propulsion is one form of feedforward

control which is able to increase exoskeleton torque with walking speed [11]. Incorporating a feedforward component into the controller design may be necessary to improve the controller's ability to adapt both torque and net work to different speeds.

Future work would also address adjusting NMM control parameters with walking speed and investigating conditions such as walking under a load and slower walking. Investigating the controller's effectiveness in different conditions, varying controller parameters with speed and adding a feedforward component may improve the controller's performance and help identify appropriate applications.

Performance of a Powered Ankle Exoskeleton Using Neuromuscular Model-Based Control over a Range of Walking Speeds

By
James V. M^{c}Call

A thesis submitted to the Graduate Faculty of
North Carolina State University
in partial fulfillment of the
requirements for the degree of
Master of Science

Biomedical Engineering

Raleigh, North Carolina

2019

APPROVED BY:

_____	_____
Dr. Derek Kamper	Dr. Gregory Sawicki
Committee Chair	

_____
Dr. Jason Franz

DEDICATION

To Anna, thank you for your love and support. We are in this together, and I wouldn't have it any other way.

BIOGRAPHY

I received my Bachelors of Science in Biomedical Engineering from North Carolina State University in 2014 graduating Cum Laude. For several years after graduation, I worked as an engineer for Robling Medical on medical device development, testing and manufacturing. During my time there, I discovered a desire to grow further as an engineer, a passion for research, and an interest in working more directly with the medical challenges many face every day. I returned to school in 2016 to pursue a Masters/PhD program in the Joint Department of Biomedical Engineering at North Carolina State University and University of North Carolina at Chapel Hill.

ACKNOWLEDGEMENTS

Anna, thank you for supporting when I decided to enter graduate school, and thank you for continuing to support me along the way. You have made this possible. Thanks to my family for sharing your love and support. Advice, encouragement, and perspective from those who have already completed graduate programs has been invaluable.

I was lucky to have the opportunity to work with Sasha Philius, another graduate student. We spent many late nights in the gait lab troubleshooting the equipment and the controller, and bouncing ideas off each other. I would also like to thank Richard Nuckols for all his work that laid the foundation for this research, and the other members of the PoWeR lab.

Dr. Jason Franz, thank you participating as a member of my committee and bringing a unique viewpoint to this project.

Dr. Gregory Sawicki, thank you giving me the opportunity to work on this project. I learned a lot from working with you and you helped make sure my first year of graduate school was a fruitful one.

Dr. Derek Kamper, you made completing this thesis possible. Thank you for accepting me into your lab and for taking the time to allow me to finish this thesis in addition to my work in the Hand Rehabilitation laboratory. I have learned and continue to learn a great deal from working with you.

TABLE OF CONTENTS

LIST OF TABLES

LIST OF FIGURES

CHAPTER 1: INTRODUCTION

1.1 Ankle Exoskeleton Application

Approximately half of the total positive work generated in a lower limb is generated about the limb's ankle joint [12]. Assistive devices can be used to supplement the users' ankle joint moments and allow them to augment their push-off capability during walking. Powered exoskeletons are one such assistive device which may improve gait of both able-bodied individuals [13] and those who suffer impairment due to neuromuscular disorders [2]. Powered ankle-foot exoskeletons typically apply torque around the ankle using one or more motors. The torque may be controlled by impedance according to stride percentage or according to the user's relevant muscle activity (i.e. myoelectric control).

1.2 Exoskeleton Control Adaptability

Effective exoskeleton control is dependent upon the interactions between the user, the device, and the environment. It is necessary for the exoskeleton controller to be capable of adapting to varying user needs (such as desired walking speed). Common exoskeleton control paradigms require parameters to be defined *a priori* or may restrict use to certain conditions.

In the past, exoskeletons have been used to reduce metabolic energy consumption but have not necessarily always been designed to quickly adapt to changing walking conditions (walking speed, ground slope, etc.) [3], [4], [14]. The ability for an exoskeleton controller to adapt to changing walking conditions is important because biological lower-

limb joints adapt their joint moments and kinematics for different walking speeds and conditions [15].

An exoskeleton was developed which was capable of decreasing metabolic expenditure after tuning the device (selection of spring stiffness, etc.) but the device was tested for only a single walking speed with level walking conditions; it was not evaluated for the wide range of conditions encountered in everyday walking [4].

One study found an optimal, though non-biological, actuation profile for ankle exoskeletons for healthy adults for minimizing metabolic expenditure [3]. This optimization process requires 120 seconds of metabolic data from steady-state walking conditions in order to identify the optimal actuation profile. Therefore, this method is not appropriate for adapting exoskeleton actuation to new conditions in real time. As the controller optimizes to continually changing conditions, the user may be hindered instead of helped by the exoskeleton.

While these studies represent successful applications of ankle exoskeletons, these examples use control mechanisms which are either tuned to a single set of walking conditions or unable to adapt to changing walking conditions quickly, even with the continuous measurement of metabolic energy consumption.

1.3 Neuromuscular Model-Based Control

Model-based control may allow for the creation of exoskeletons that can adapt to changing demands in real time and without user input. Neuromuscular model-based (NMM) control aims to estimate the force produced by a biological muscle or set of

biological muscles by using joint angle as an input into a Hill-type muscle model. The model calculates muscle force based on force-length, and force-velocity relationships. As the exoskeleton user moves, the joint angle changes and acts as an input into the controller. The controller adapts to changing walking conditions by mimicking the biological muscle's estimated behavior.

Past studies have examined the performance of an NMM-controlled unilateral powered ankle-foot prosthesis based on plantar flexor behavior. The controller virtually emulated a Hill-type muscle model with positive force feedback. The results demonstrated normalized energetics and mechanics for amputees across a range of walking speeds and ground slopes, indicating that this control strategy would allow adaptation between varied walking conditions [5], [6].

Two studies in the past have used NMM controllers to simulate walkers [9], [10]. In these two studies, NMM control was successfully used to simulate walkers over a range of walking speeds (of 0.4 – 1.35 ms^{-1}) when a feedforward component was included in the controller.

Two studies have used NMM controllers to control exoskeletons [7], [8]. One study used a NMM controller with a hip and knee exoskeleton for patients with SCI, and was able to modulate exoskeleton torque across a range of walking speeds [8]. The other study used an NMM controller to control bilateral ankle exoskeletons across a range of slow walking speeds [7]. This study found slight decreases in metabolic energy consumption due to exoskeleton torque but only included results from two participants.

These past studies yielded some promising results, but did not address high walking speeds and included a very limited examination of the impact of NMM controllers on metabolic energy consumption. Only one of these studies looks at the use of NMM control for ankle exoskeletons and takes measurements of metabolic energy consumption, but this study had a very limited sample size [7]. Additionally, none of the past studies examined high walking speeds (typically 1 ms^{-1} or less).

1.4 NMM Control – High Walking Speed

The aim of this study was to evaluate an NMM controller for bilateral powered ankle-foot exoskeletons when used during treadmill walking at several different speeds. I hypothesized that the exoskeleton controller would increase torque and positive work as walking speed increased and reduce metabolic energy consumption at all walking speeds. As walking speed increases, biological moment at lower-limb joints is increased and metabolic cost increases [15]. I expected that as speed increased, net work and exoskeleton torque would increase as well and the torque and work would reduce metabolic energy consumption across speeds. The goal of this study was to determine the capabilities of a NMM-controlled exoskeleton and its adaptation to different speeds. Results revealed that this type of controller may be less effective at high walking speeds and may require additional inputs to operate appropriately in a larger range of conditions.

New knowledge from this study can help determine how an NMM controller can be used to assist individuals with intact limbs at typical walking speeds.

CHAPTER 2: METHODS

2.1 Tethered Bilateral Ankle Exoskeleton Testbed

An exoskeleton emulator [16] provided participants with bilateral torque assistance at the ankles. Carbon fiber ankle foot orthoses (AFO) were attached to the participants' shoes and calves/shins. Each AFO had a rotational joint, which was axially aligned with the ankle. Variations in participant geometry were accommodated by having a range of sizes for the carbon fiber components and by adjusting the AFO joint position. The AFOs were tethered to off-board motors (Baldor Electric Co, Fort Smith, AR) that generated torque around the ankles via a Bowden-cable transmission system. A goniometer (500 Hz, Biometrics, UK) was used on each AFO joint to measure real-time ankle angle. Applied torque was calculated using the moment arm of each AFO and cable force measured with a load cells (500 Hz, LCM Systems Ltd, UK) placed in series with the Bowden. Control and signal I/O were handled by a real-time computer (500 Hz, dSPACE, Germany). The exoskeleton emulator was used in conjunction with an instrumented treadmill (BERTEC, Columbus, OH, USA) so that trials could be performed at fixed speeds.

2.2 Exoskeleton NMM Controller

Neuromuscular model-based control of an exoskeleton is the idea that Hill's relationships of force and length and shortening velocity can be used in combination with reflex-based feedback to estimate the force being produced by a MTU in real time. The Hill-type muscle model models a muscle tendon unit as a combination of two elements: the tendon is modeled as a series elastic element (SEE); the muscle is modeled as a contractile element, which also has passive elastic properties (CE) [17]. By measuring the ground

reaction force to determine the phase of gait (stance or swing), and by measuring ankle angle it is possible to estimate the torque currently being generated about the ankle.

Measuring ankle angle allows for estimation of MTU length change and its shortening velocity (**Eqn. 1.1 and 1.2**). The NMM controller used here was feedback based and had no feedforward component. The primary input was the ankle angle. Past studies have suggested adding feedforward components to NMM controllers, such central pattern generator components, in order to improve adaptability of NMM controllers, especially in regards to speed adaptation [10]. However, we did not include any feedforward components in this controller. Pure feedforward exoskeleton controllers (e.g., proportional myoelectric propulsion) have been studied in the past [11], and we, similarly, chose to study the performance of a pure NMM controller. A NMM controller with no feedforward component has fewer control inputs, and requires less individual tuning for each participant than an NMM controller with a feedforward component.

The neuromuscular model was designed in Simulink (MathWorks, USA) as a force feedback reflex-based controller, similar to the controller used in Eilenberg et al. [5] A Hill-type muscle model was used for the emulated plantar flexor tendon unit (MTU). The model included a contractile element (CE) with active and passive properties and a series elastic element (SEE). Internal states of the MTU model (**Figure 1**) were calculated with the length of the MTU as a function of modeled musculoskeletal geometry and ankle angle (**Figure 1**) (**Eqn. 1.1**). CE length and velocity were subject to force-length, force-velocity, and activation dynamics (**Eqn. 1.2**). Hill was able to determine relationships between force produced by a muscle and its length relative to its resting length (**Eqn. 1.8 and 1.9**) (whether

shortened or stretched), and between force produced and the muscle's shortening velocity (**Eqn. 1.10 and 1.11**). SEE length was calculated as the difference between the MTU and CE lengths (**Eqn. 1.3**). The ankle angle was measured and used to determine the length of the MTU. Previous CE lengths and activation were used with force-length and force-velocity relationships to determine the CE contraction velocity. CE velocity was used to find the current CE length. MTU and CE length were used to find SEE length. SEE length was directly related to MTU force. Characteristics of the MTU were obtained from models that combined the characteristics of the gastrocnemius and soleus muscles [5], [18]–[25].

$$L_{MTU} = f\left(\theta_{ank}, r_{ank}\right) \tag{1.1}$$

$$\dot{L}_{CE} = f\left(\text{F-L}, \text{F-V}, a\right) \tag{1.2}$$

$$L_{SEE} = L_{MTU} - L_{CE} \tag{1.3}$$

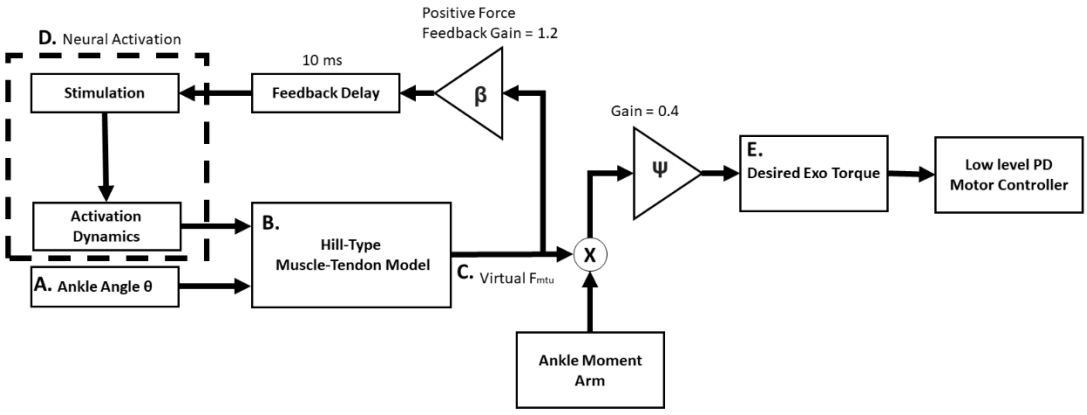

Figure 1. NMM controller block diagram. (A) Ankle angle and (B) a Hill-type MTU model is used to estimate internal states and output of a virtual MTU. (C) Virtual MTU force creates a positive force feedback (β) signal (Gain = 1.2) that is delayed by 10 ms and then enhances (D) neural activation. A gain (ψ) of 0.4 is applied to the virtual ankle moment to calculate the desired assistance to be supplied by the exoskeleton (E).

MTU force **(**F_{MTU}**)** (**Figure 1**) was a function of the model's SEE stiffness and strain (**Eqn. 1.3 and 1.12**). In the reflex pathway, F_{MTU} was normalized to F_{max}, a feedback gain of 1.2 was applied, and a 10ms delay was added to emulate a positive force feedback neural signal (**Figure 1**). CE activation dynamics (ACT) were modeled in order to close the feedback loop.

Desired exoskeleton torque was calculated as a percentage of estimated virtual biological moment using **Eqn. 1.4** where ψ represented a percentage of the estimated biological moment. We used a gain of 0.4.

$$\tau_{exo} = F_{MTU} \times r_{ankle} \times \psi \tag{1.4}$$

2.2.1 Activation Dynamics Time Constants

Time constants for activation dynamics (τ_{act} = 0.033 s, τ_{dact} = 0.091 s) were obtained from a MTU model which combined the characteristics of the soleus and gastrocnemius muscles [18]–[20]. In the NMM controller, this equation was run and recalculated at a rate of 500 Hz.

Activation Dynamics:

$$\alpha(t) \; : \; \int [\left(\frac{u(t)}{\tau_{act}}\right) - \left(\frac{1}{\tau_{act}}\right) \; * (\beta + (1-\beta) * u(t))] dt, \; \beta = \tau_{act/} \, \tau_{dact} \tag{1.5}$$

2.2.2 Neural Stimulation Equation

The equation for determining neural stimulation was obtained from a study investigating a positive force feedback model [21]. In the NMM controller, this equation was run and recalculated at a rate of 500 Hz.

Neural Stimulation:

If t > 10 ms, u(t) : $u_0 + G_{FB} * F_{mtu}(t - 10ms)/F_{max}$, u_0 = 0.01, G_{FB} = 1.2 (1.6)

If t =< 10, u(t) : u_0, u_0 = 0.01 (1.7)

2.2.3 Controller Feedback Gain

A feedback gain of 1.2 was applied in the NMM controller. This value was determined from the optimized set of NMM controller values reported in Eilenberg et al. 2009 [5]. The feedback value was determined by a genetic algorithm optimizing several parameters to try to match model-produced torque profiles with biologically produced torque profiles at a walking speed of 1 ms^{-1}.

2.2.4 Controller Reflex Delay

In Eilenberg et al. 2009, a reflex delay of 20 ms was chosen for delaying the neural stimulation signal. In the NMM controller we created, this delay was reduced to 10 ms after experimentation with different delay lengths while tuning the exoskeleton prior to beginning data collection.

2.2.5 Controller Torque Gain

Unlike a prosthesis which may be intended to entirely replace biological moment, the goal was to only supplement biological torque and power at the ankle with a parallel ankle exoskeleton. A past NMM-controlled exoskeleton investigation found conflicting results between two subjects on whether a gain of 0.5 or 1.0 on the estimated biological torque was better [7]. In Collins et al. [4] and in Takahashi et al. [26] the peak exoskeleton

torque used was about 25% of biological torque. In a hip and knee exoskeleton NMM controller study for SCI patients, gains of between 0.3-1.0 were used [8]. A range of gains from 0.25-0.60 was piloted, and it was found that for gains higher than 0.40, participants had difficulty controlling the exoskeletons at high walking speeds. I chose to use a gain of 0.40, as it was the highest gain possible that I expected would still allow for comfortable walking at all speeds used in the study.

2.2.6 Controller MTU Maximum Force

Maximum MTU Force (F_{max} = 6000 N) was obtained from a MTU model which combined the characteristics of the soleus and gastrocnemius muscles [19], [22].

2.2.7 Controller CE Force-Length and Force-Velocity Equations and Constants Gain

Force-Length and Force-Velocity relationships and constants were obtained from a MTU model which combined the characteristics of the soleus and gastrocnemius muscles [19], [23], [24]. The combined active and passive force-length relationships cause potential muscle force to generally increase as CE length increases. The CE active force-length relationship has potential muscle force increase as the muscle lengthens until the optimal length is achieved, and then the potential force decreases. The CE passive force-length relationship increases CE force as length increases past the optimal CE length. The force-velocity relationship causes potential muscle to decrease as muscle contraction velocity increases.

Muscle Force-Length:

F_l active: $e^{-\left|\frac{\left(\frac{l_m}{l_0}\right)^b-1}{s}\right|^a}$, b=0.8698, s= 0.3914, a = 3.1108 (1.8)

F_l passive: $A * e^{b*(\frac{l_m}{l_0})-1}$, A= 0.0238, b= 5.31 (1.9)

Muscle Force-Velocity:

F_v when $V_m > 0$: $(1-(\frac{V_{CE}}{V_{max}}))/(1+\left(\frac{V_{CE}}{k*V_{max}}\right))$, k=0.17 (1.10)

F_v when $V_m < 0$: $1.8-0.8*((1+\frac{V_{CE}}{V_{max}})/(1-7.56*\left(\frac{V_{CE}}{k*V_{max}}\right))$, k=0.17 (1.11)

2.2.8 Controller Tendon Stiffness Equation and Constants

The tendon stiffness relationship and constant were obtained from MTU models which combined the characteristics of the soleus and gastrocnemius muscles [19], [25].

Tendon Stiffness:

K_{SEE} : $k_t * (1+(0.9/-e^{(Q*F_{CE})/F_{max}})$, Q = 20, k_t=315.4 N/mm (1.12)

2.2.9 Controller CE and SEE constants

The maximum CE contraction velocity (Vmax = 0.326 ms^{-1}), CE optimal length (CE L_0 = 0.04 m) , SEE slack length (SEE L_0 = 0.326 m) were obtained from a MTU model which combined the characteristics of the soleus and gastrocnemius muscles [25].

2.3 Experimental Protocol

2.3.1 Participants

Eight able-bodied participants (6 male), capable of walking without assistance, consented to participate in this study (mean ± s.d., age = 23.5 ± 3.2 years; mass = 69.5 ± 5.3 kg; height = 1.75 ± 0.05 m). Characteristics for individual participants are listed in ***Table 1***.

Table 1: NMM Study Participant Data

Participants	**Sex**	**Age** (years)	**Mass** (kg)	**Height** (meters)
1	M	26	71.8	1.75
2	M	29	72.7	1.78
3	M	24	75.8	1.73
4	M	23	65.9	1.80
5	F	25	73.1	1.68
6	M	18	59.9	1.80
7	M	23	73.5	1.78
8	F	20	63.3	1.68
Mean ± SD	**6 M**	**23.5 ± 3.2**	**69.5 ±5.3**	**1.75 ± 0.05**

2.3.2 Procedure

Each walking trial lasted for seven minutes and was completed on the instrumented treadmill. Each participant completed a training day where they walked on the treadmill at 1.25 ms^{-1} in the exoskeleton AFOs. They walked without assistance for 5 minutes and then walked with exoskeleton assistance (modulated by the NMM controller) for 20 minutes. Data was collected on a second day at least 48 hours after the completion of the training day.

Each participant walked on the treadmill for nine different conditions, each determined by the combination of two factors: walking speed (1.25 ms^{-1}, 1.50 ms^{-1}, 1.75 ms^{-1}), and exoskeleton status (No exoskeleton, exoskeleton - unpowered, exoskeleton - powered) (**Figure 2**). Values for walking speeds were based on a range of high walking speeds for able-bodied adults. A safety harness was worn to decrease risk of falls or injuries. The treadmills were equipped with handrails, but participants were instructed only to use these for balance corrections as needed. Under normal operation the safety harness did not support body weight.

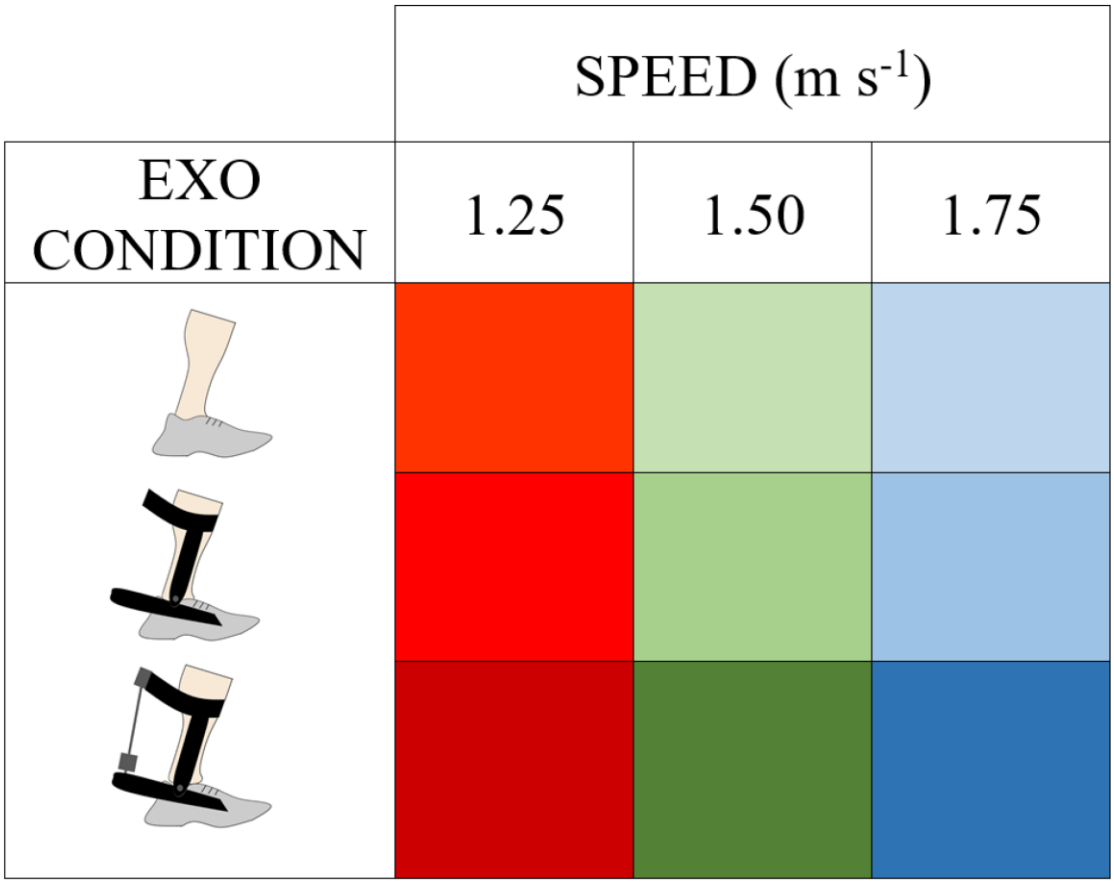

Figure 2. Walking Speed and Exoskeleton Parameters. Data were collected during nine walking trials for each participant. Each participant walked at the same three walking speeds while: not wearing an exoskeleton, while wearing an unpowered exoskeleton, and while wearing a powered exoskeleton. The shade and color-coding scheme in this figure, used to indicate walking trial, was used in figures throughout this document. The color (red, green, blue) indicates the respective walking speed (1.25 ms-1, 1.50 ms-1, 1.75 ms-1). The shade indicates whether an exoskeleton was present and active (darkest shade), inactive (medium shade), or not present (lightest shade) during the trial (lightest shade, darker shade, darkest shade).

2.4 Outcome Measures

2.4.1 Metabolic Energy Consumption

Metabolic energy consumption during trials was estimated via indirect calorimetry. Oxygen and carbon dioxide flow rates into and out from the lungs were measured using a portable system (OXCY MOBILE, VIASYS Healthcare, Yorba Lina, CA, USA) and these flow rates were converted to metabolic power using the Brockway equation [27]. Data were collected for the duration of each trial; data from the last two minutes of each seven-minute trial were used as a representative sample of the metabolic energy consumption rate (metabolic energy consumption rate stabilized in the first five minutes of each trial). Data obtained from the last two minutes of a five-minute standing trial were averaged to estimate the participants' basal metabolic energy consumption rate. The basal metabolic rate was subtracted from the average rate from each trial and the result was normalized to the participant's body mass (W kg ms^{-1}).

2.4.2 Biomechanics

Anthropometric data (height, weight, measurements of lower limbs and feet, etc.) were collected for each participant before beginning testing. Reflective markers were placed at the joints and on body segments to be used with an eight-camera motion analysis system (120 Hz, VICON, Oxford, UK). The markers were placed on each leg/foot (when applicable) in the following locations: four marker rigid plate on the pelvis, anterior superior iliac crests, greater trochanters, four marker rigid plate on the thighs, medial and lateral epicondyles of the knee, four marker rigid plate on the shanks, medial and lateral malleoli

of the ankle, third metatarsophalangeal joint of the toe, four marker rigid plate on the feet and posterior calcaneus of the heel.

A seven-segment model composed of two thighs, two shanks, two feet and one pelvis was calibrated using a static standing trial. A second-order low pass Butterworth filter (10 Hz cutoff) was used to filter marker positions. Joint angles were computed using the orientation of the distal segment with respect to the proximal segment. Inverse dynamics was used to compute joint moments. The product of joint moments and joint angular velocity yielded power at the joint. Joint work rate was calculated as the integral of joint power over the period of positive or negative work divided by stride time. In trials where an exoskeletal torque was applied, the biological ankle joint moment was calculated by subtracting the measured exoskeleton torque from the total joint torque, calculated using inverse dynamics.

2.4.3 Electromyography

Muscle activity of the medial gastrocnemius (MG) and lateral gastrocnemius (LG), lateral portion of the soleus (SOL), and the tibialis anterior (TA) of the right leg were measured using surface electromyography (sEMG). Wired electrodes (SX230, Biometrics Ltd., Newport, UK) were used to collect the signals, which were sampled at a frequency of 960 Hz. The signals were high-pass filtered with a cutoff frequency of 6 Hz, rectified, and low-pass filtered with a cutoff frequency of 20 Hz.

2.4.4 Data Analysis

Comparisons were made across test conditions for metabolic rate, joint mechanics, and muscle activity. Average trajectories were created for each subject and then normalized to percent stride. Metabolic rate and joint mechanics were normalized to body mass, while muscle activity measurements were normalized to peak activation for each muscle. Outcomes were averaged across subjects; standard deviations represent variations between subjects.

Primary statistical analysis was performed using repeated-measures ANOVA with a Bonferroni adjustment to test for significant trends in average exoskeleton torque, average exoskeleton positive work, average biological torque, average biological positive work, and average metabolic energy consumption rate. Paired T-tests with Bonferroni adjustment were used to determine statistical difference between conditions. P-values less than 0.05 were considered significant and were reported.

Secondary statistical analysis was performed using repeated-measures ANOVA without Bonferroni adjustment to test non-primary variables for trends. Paired T-tests without Bonferroni adjustment were used to determine statistical difference. P-values less than 0.05 were considered significant and were reported.

CHAPTER 3: RESULTS

3.1 Results Summary

Exoskeleton work rate did not significantly change as walking speed increased, although exoskeleton average torque was significantly reduced at the highest walking speed compared to the lowest walking speed. Peak exoskeleton torque did not significantly change with walking speed. There were significant reductions in positive and negative average biological work rate, positive and negative peak biological work rate, average biological torque and peak biological torque in the powered condition compared to the unpowered condition.

The virtual activation state of the controller saw significant reduction (-34%) as speed increased from 1.25 ms^{-1} to 1.75 ms^{-1}. Controller MTU force consistently decreased as walking speed increased (-24%). Ankle plantarflexion increased and stride time decreased with walking speed in the powered condition.

Metabolic energy consumption rate during powered exoskeleton trials compared to unpowered exoskeleton trials was not significantly different at any speed.

3.2 Exoskeleton and Biological Work and Torque

Positive work rate for the exoskeleton did not change significantly with walking speed, while negative exoskeleton work rate significantly increased with walking speed. Negative biological work rate was reduced at all speeds in the powered condition compared to the unpowered condition. **Figure 3** and **Figure 4** show biological and exoskeleton work rate for all conditions, and power for all conditions over percent stride.

Primary analysis (Bonferroni adjusted) two-way repeated measures ANOVA testing found main effects and interactions for the following torque and work rate measurements: average exoskeleton torque (walking speed, $p = 0.04$); average biological torque (walking speed, $p = 0.005$); biological average positive work rate (walking speed, $p = 0.005$).

Secondary analysis (non-Bonferroni adjusted) two-way repeated measures ANOVA testing found main effects and interactions for the following torque and work rate measurements: exoskeleton peak negative work rate (walking speed, $p = 0.016$); peak biological torque (exoskeleton power, $p = 0.001$; walking speed, $p = 0.001$); biological average negative work rate (exoskeleton power, $p = 0.003$); biological peak positive work rate (exoskeleton power, $p = 0.020$; walking speed, $p = 0.001$).

The powered condition had a significantly increased exoskeleton negative work rate at 1.75 ms^{-1} compared to at 1.50 ms^{-1} ($p=0.045$), and at 1.75 ms^{-1} compared to at 1.25 ms^{-1} ($p=0.036$). Peak positive and negative work rates produced by the exoskeleton did not significantly change with speed. Positive biological work rate in the powered condition compared to the unpowered condition was not significantly reduced (-10.0% at 1.50 ms^{-1} ($p = 0.055$), and -8.4% at 1.75 ms^{-1} ($p =0.100$)). Negative biological work rate in the powered condition compared to the unpowered condition was reduced by 37.8% at 1.25 ms^{-1} ($p = 0.001$), 31.9% at 1.50 ms^{-1} ($p = 0.010$), and 32.3% at 1.75 ms^{-1} ($p =0.013$). Peak positive biological work rate in the powered condition compared to the unpowered condition was reduced by 15.7% at 1.25 ms^{-1} ($p = 0.043$), 22.1% at 1.50 ms^{-1} ($p = 0.009$), and 16.9% at 1.75 ms^{-1} ($p =0.042$). Peak negative biological work rate in the powered condition compared to

the unpowered condition was significantly reduced by 21.1% at 1.25 ms^{-1} ($p = 0.018$), and 22.9% at 1.75 ms^{-1} ($p = 0.049$).

As walking speed increased, peak exoskeleton generated torque did not change by a significant amount (**Figure 3**), and peak biological torque decreased in the powered condition compared to the unpowered condition across speeds by 12.0% at 1.25 ms^{-1} ($p = 0.006$), 7.2% at 1.50 ms^{-1} ($p = 0.001$), and 11.3% at 1.75 ms^{-1}s ($p = 0.001$) (**Figure 4**). Average biological torque in the powered condition compared to the unpowered condition was reduced by 10.9% at 1.75 ms^{-1} ($p = 0.001$). Average exoskeleton torque at 1.75 ms^{-1} was reduced by 16.4% ($p = 0.019$), in comparison with average exoskeleton torque at 1.25 ms^{-1}, as speed increased.

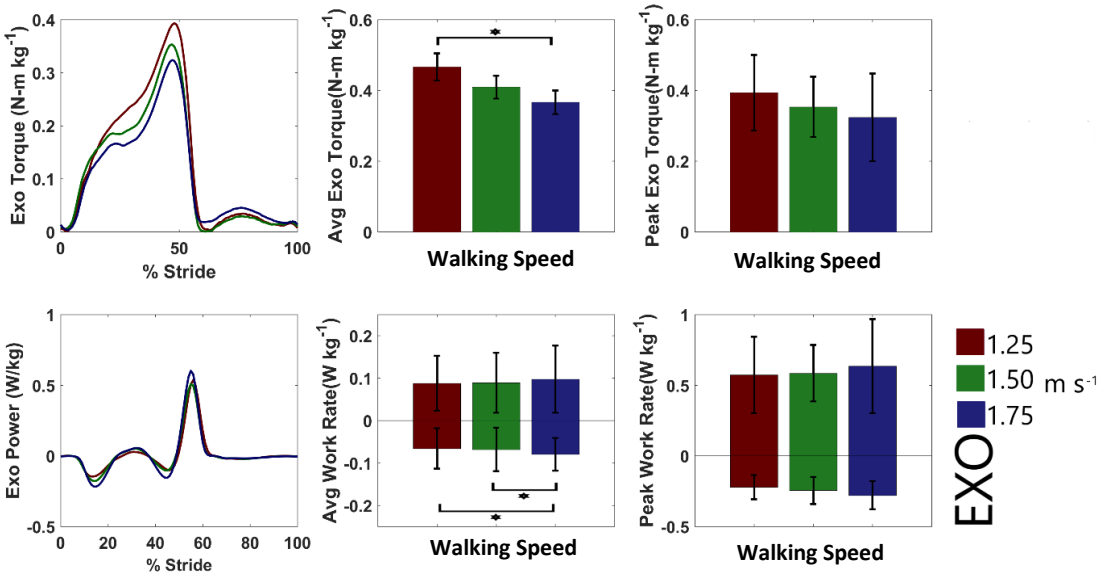

Figure 3. Exoskeletal Power and Torque. The values for exoskeleton torque and work rate during the three powered walking trials are averaged from all eight participants, and normalized to average participant mass. The left two panels display the exoskeleton torque and power across percent stride. The center two panels display the average exoskeleton torque, and average positive and negative exoskeleton work rate. The right two panels display the peak torque, peak positive work, and peak negative work. * $p < 0.05$

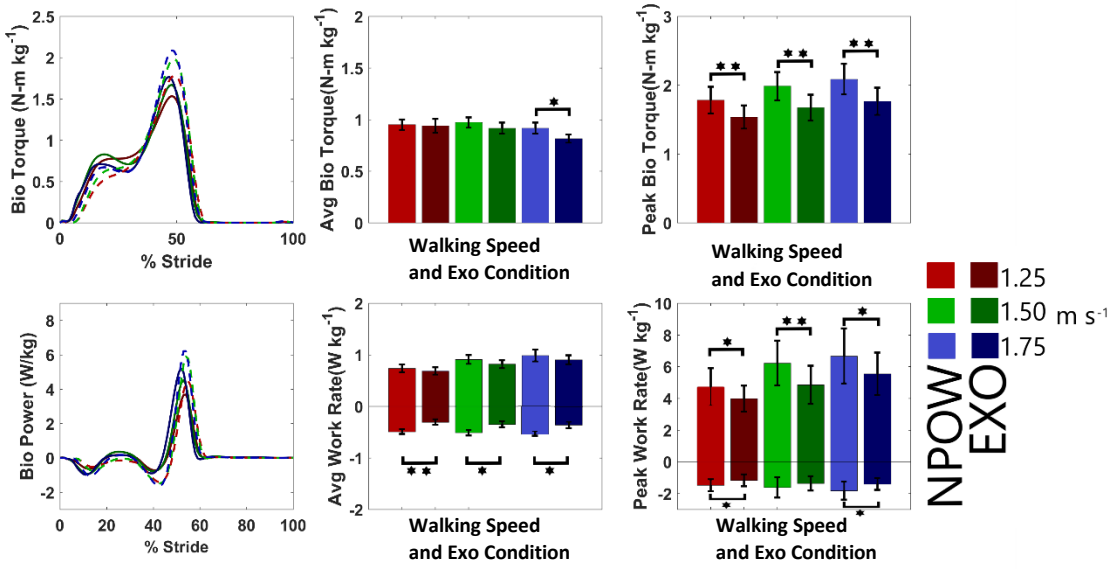

Figure 4. Biological Torque and Power. The values for the biological ankle torque and work rate during the three powered exoskeleton and three unpowered exoskeleton walking trials are averaged from all eight participants, and normalized to average participant mass. The left two panels display the biological torque and power across percent stride. The center two panels display the average biological torque, and average positive and negative biological work rate. The right two panels display the peak torque, peak positive work rate, and peak negative work rate. * $p < 0.05$; ** $p < 0.01$

3.3 Kinematics

Secondary analysis (non-Bonferroni adjusted) two-way repeated measures ANOVA testing found main effects and interactions for the following kinematic measurements: peak dorsiflexion of the ankle (walking speed, $p = 0.038$); peak plantarflexion of the ankle (exoskeleton power, $p = 0.001$; walking speed, $p = 0.011$). Walking with the exoskeleton in the powered condition significantly increased peak plantar flexion by 4.1 degrees at 1.25 ms^{-1} ($p=.001$), 2.43 degrees at 1.50 ms^{-1} ($p=.001$), and 4.9 degrees at 1.75 ms^{-1} ($p=.006$). It also significantly decreased peak dorsiflexion by 7.5 degrees at 1.75 ms^{-1} ($p=.045$), compared to walking in the unpowered condition. Additionally, as walking speed increased, the peak plantarflexion during pushoff increased and peak dorsiflexion decreased, in both the powered and unpowered conditions (**Figure 5**). Stride time decreased significantly as walking speed increased (1.08 s/stride at 1.25 ms^{-1}, 0.99 s/stride at 1.50 ms^{-1}, 0.91 s/stride at 1.75 ms^{-1}). Stride time during 1.50 ms^{-1} walking decreased 8.3% compared to stride time at the slowest walking speed ($p=0.001$). Stride time during 1.75 ms^{-1} walking decreased by 15% compared to the slowest walking speed ($p=0.001$), and 7.0% compared to stride time at 1.50 ms^{-1} ($p=0.001$).

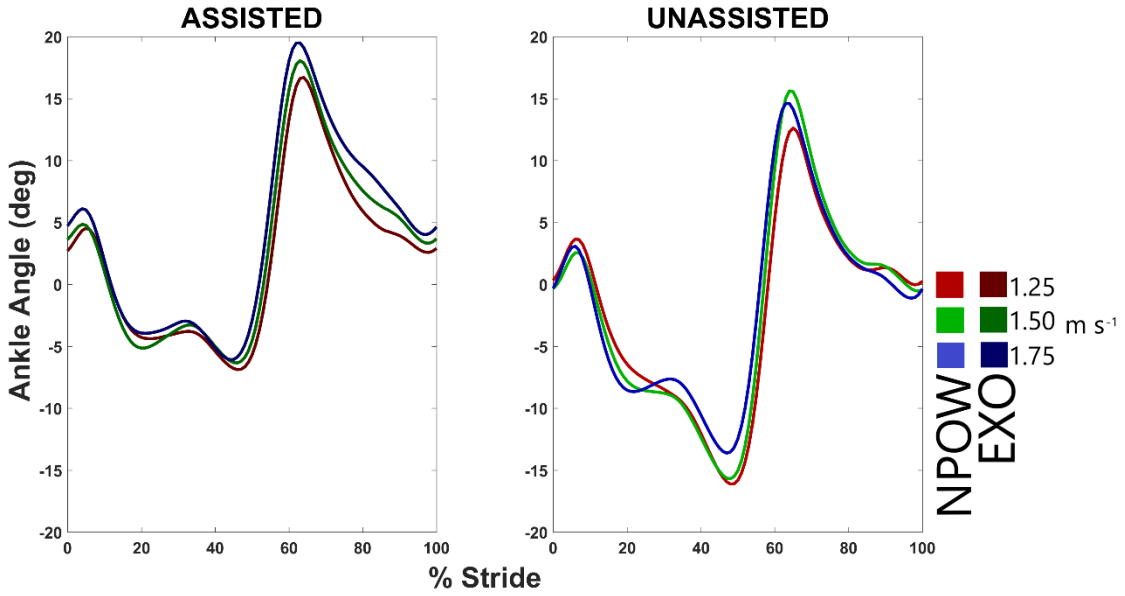

Figure 5. Impact of Exoskeleton Condition and Gait Speed on Ankle Kinematics. The values of the ankle angle over percent stride across speeds in the powered (assisted) exoskeleton condition (left panel), and the unpowered (unassisted) exoskeleton condition were averaged from all eight participants. 0% stride represents heel strike. An angle of zero degrees represents that the ankle was in a neutral position (neither plantarflexed nor dorsiflexed). A positive angle represents that the ankle was plantarflexed, and a negative angle represents dorsiflexion.

3.4 NMM Controller Internal States

Virtual muscle activation decreased significantly as walking speed increased. In the powered condition virtual activation decreased by an average of 34.8% ($p = 0.001$) as speed increased from 1.25 ms^{-1} to 1.75 ms^{-1} (**Figure 6**). Similarly, virtual MTU force production in the powered condition decreased by an average of 24.3% ($p=0.003$) (**Figure 6**) as speed increased from 1.25 ms^{-1} to 1.75 ms^{-1}. Contraction velocity of the CE did not significantly change as walking speed increased (**Figure 8**). However, there was change in CE length contraction (+10.3%), peak MTU length change (+36.7%) and SEE length (+17.1%) at the lowest walking speed compared to the fastest walking speed (**Figure 7**, **Figure 8**).

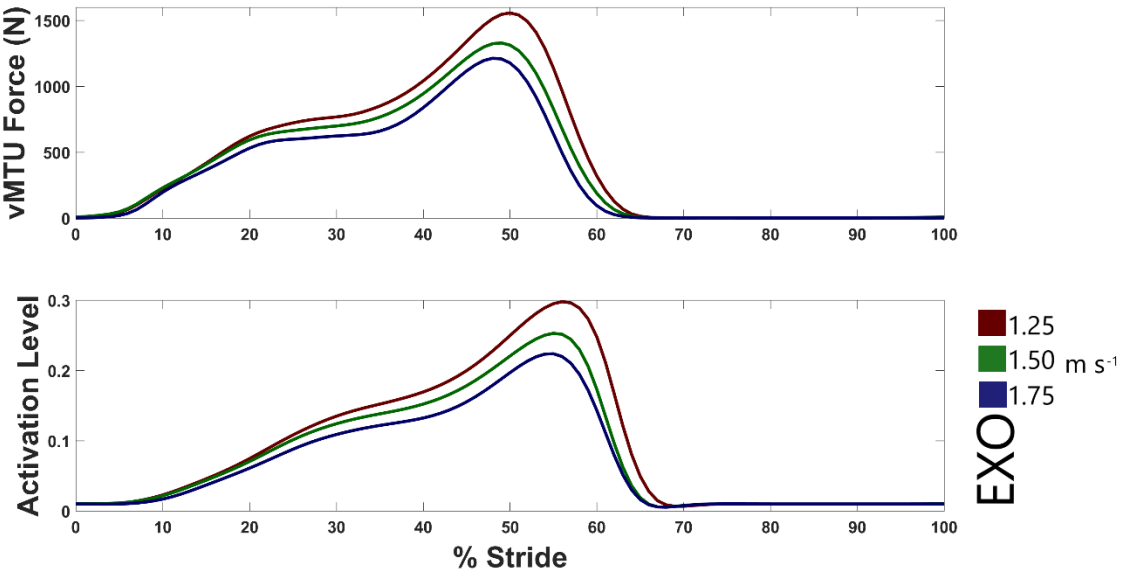

Figure 6. Controller Internal States: Virtual MTU, Virtual Muscle Activation. The values for virtual MTU force (top panel) and virtual activation level (bottom panel), within the controller at different walking speeds in the powered exoskeleton condition over percent stride, are averaged from all eight participants. Virtual MTU force and activation decreased, by 24.3% and 34.8% respectively, between the slowest and fastest walking speeds.

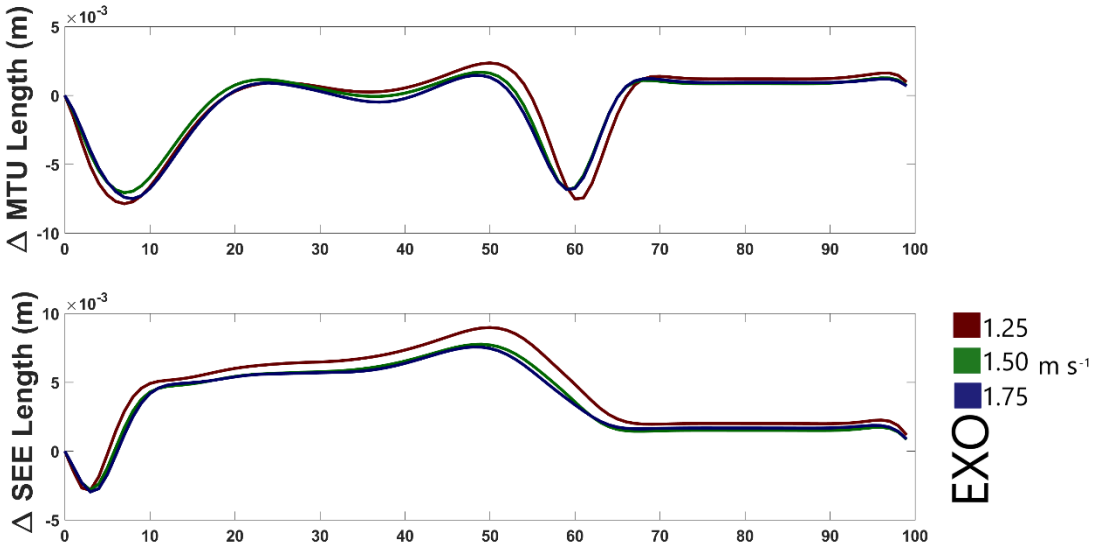

Figure 7. Controller Internal States: MTU and SEE Length Changes. The values for the virtual MTU length change (top panel) and virtual SEE length change (bottom panel) within the controller at different walking speeds in the powered exoskeleton condition over percent stride are averaged across all eight participants. Average virtual SEE length change decreased from the slowest walking speed to the fastest walking speed by 17.1% (t-test: $p = 0.006$). Peak positive MTU length change decreased from the slowest walking speed to the fastest walking speed by 36.7%, and peak negative MTU length change decreased from the slowest walking speed to the fastest walking speed by 4.6%.

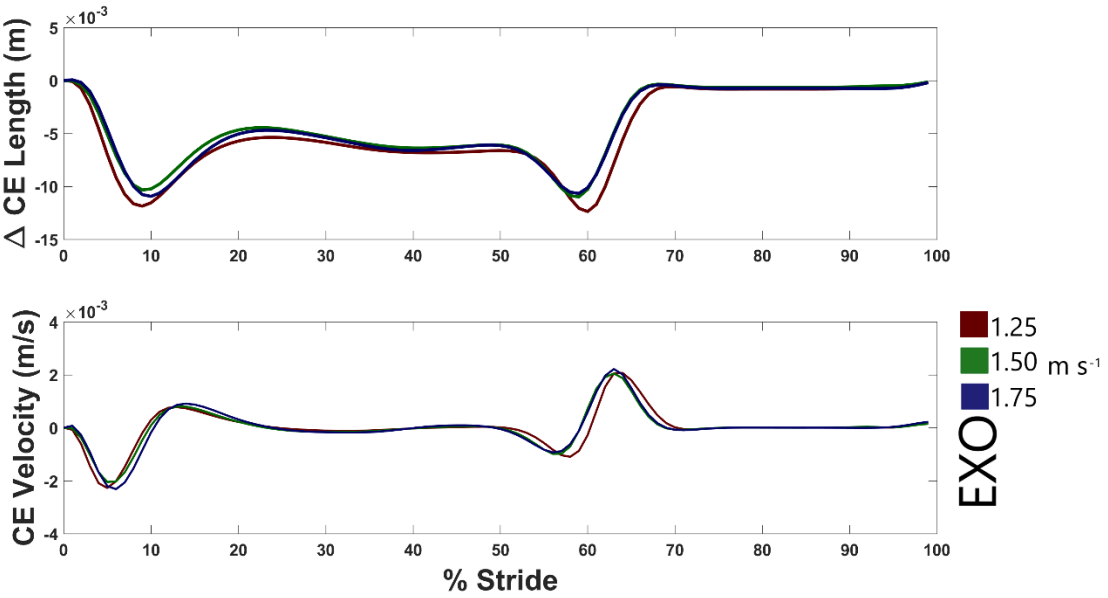

Figure 8. Controller Internal States: CE Length Change and CE Contraction Velocity. The values for the virtual CE length change (top panel) and virtual CE contraction velocity length change (bottom panel) within the controller at different walking speeds in the powered exoskeleton condition over percent stride are averaged across all eight participants. CE contraction velocities were not significantly different across walking speeds, but we do see a greater decrease (+10.3%) in CE length at the lowest walking speed compared to the fastest walking speed in the first 10% of stride.

The peak vMTU force and MTU length change decreased as gait speed increased, leading to smaller virtual MTU workloops (**Figure 9**). This means that a smaller amount of work was performed by the exoskeleton during each individual step.

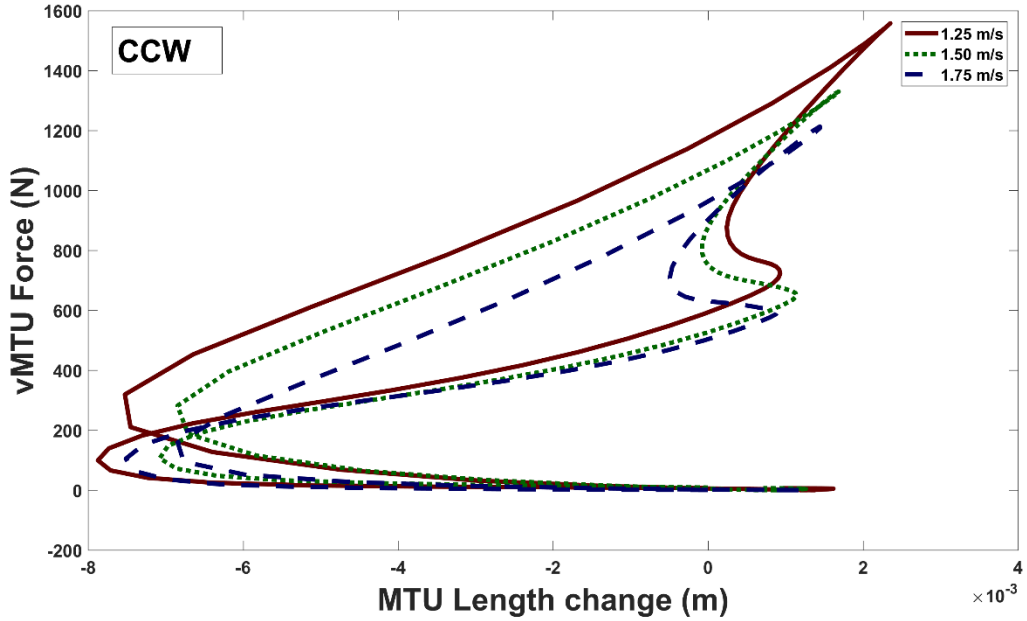

Figure 9. Virtual Muscle Workloops. Values for the work loops of the NMM controller using the virtual MTU force and the virtual MTU length change at different walking speeds were averaged from all eight participants. As walking speed increased the virtual MTU force decreased and the MTU length change decreased, causing smaller work loops. This indicates that a smaller amount of work was performed by the exoskeleton during each step as speed increases.

3.5 Metabolic Energy Consumption

Primary analysis (Bonferroni adjusted) two-way repeated measures ANOVA testing found main effects and interactions for the following metabolic measurement: metabolic energy consumption (walking speed, $p = 0.005$). The metabolic rate varied with walking speed. Metabolic rate did not change significantly in the powered condition compared to the unpowered condition across walking speeds (**Figure 10**). The metabolic rate for 1.25 ms^{-1} with powered exoskeleton trial saw a 0.2% decrease compared to the 1.25 ms^{-1} unpowered exoskeleton condition. The metabolic rate for 1.50 ms^{-1} powered exoskeleton trial saw a 3.1% increase compared to the 1.50 ms^{-1} unpowered exoskeleton condition. The metabolic rate for 1.75 ms^{-1} with powered exoskeleton trial saw a 2.9% increase compared to the 1.75 ms^{-1} unpowered exoskeleton condition. Average metabolic energy consumption rate was lowest in the no exoskeleton condition at every walking speed.

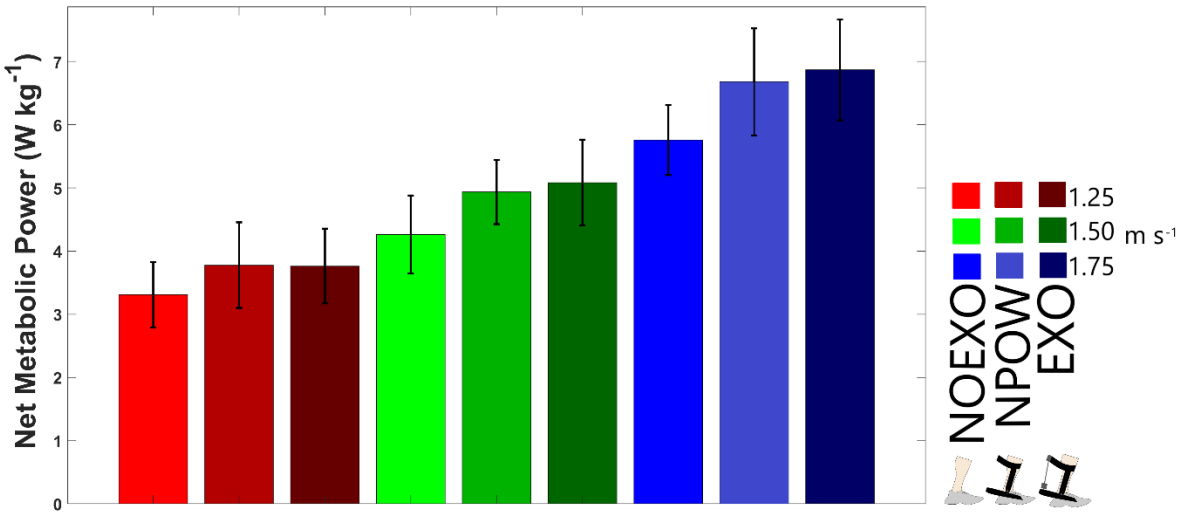

Figure 10. Metabolic Energy Consumption Rate. Values for the metabolic power consumption during all nine walking trials were averaged from all eight participants. Metabolic power consumption was determined using the volume of O2 and CO2 inhaled and exhaled during the last two minutes of each trial, and then calculating metabolic energy using the Brockway equation. The values reported represent the difference between metabolic power consumption during each condition and the basal metabolic energy consumption rate found during a five minute standing trial.

3.6 Electromyography

Secondary analysis (non-Bonferroni adjusted) two-way repeated measures ANOVA testing found main effects and interactions for the following EMG measurements: EMG averaged across all four muscles (exoskeleton power, p = 0.008; walking speed, p = 0.001); peak EMG averaged across all four muscles (walking speed, p = 0.001); average MG EMG (exoskeleton power, p = 0.003; walking speed, p = 0.001); average TA EMG (exoskeleton power, p = 0.003; walking speed, p = 0.001).

Average EMG averaged across all four muscles (MG, LG, SOL, and TA) was significantly increased between the powered and unpowered condition across speeds (21.5% at 1.25 ms^{-1} (p=0.031), 13.1% at 1.50 ms^{-1} (p=0.019), and .9% at 1.75 ms^{-1} (p=0.028)) (**Figure 11**). Peak EMG averaged across all four muscles (MG, LG, SOL, and TA) was not significantly different between the powered and unpowered condition across speeds (**Figure 11**). Peak EMG amplitude of the MG in the powered condition is significantly reduced at the lowest walking speed compared to the unpowered condition (-15.5% at 1.25 ms^{-1} (p=0.014)). Average TA co-activation increased in the powered condition compared to the unpowered condition across speeds (35.5% at 1.25 ms^{-1} (p=0.026), 48.6% at 1.50 ms^{-1} (p=0.01), and 15.8% at 1.75 ms^{-1} (p=0.026)).

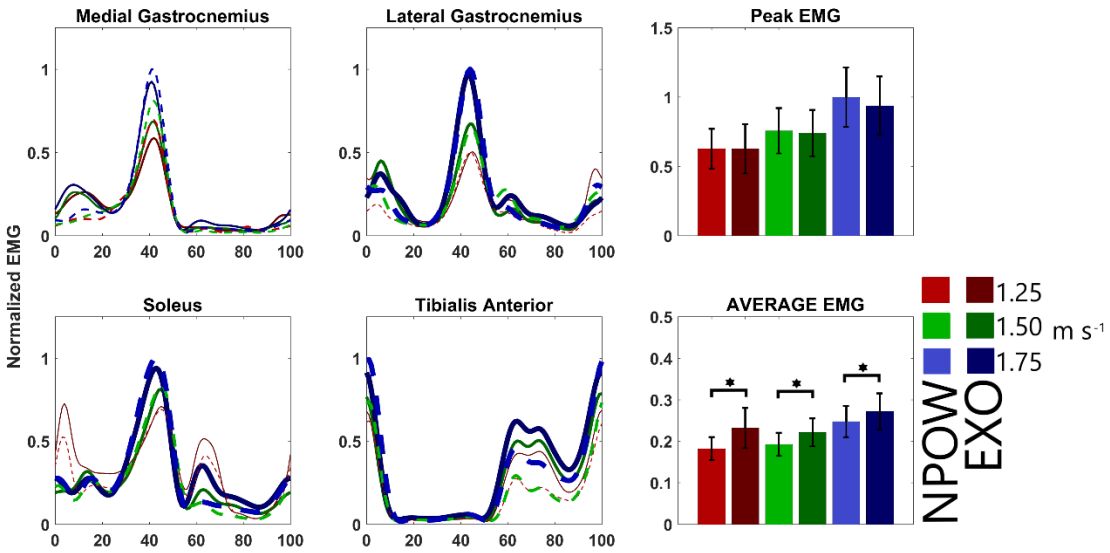

Figure 11. Normalized EMG. Values for EMG signals sampled during the six powered exoskeleton and unpowered exoskeleton walking trials are averaged from all eight participants. EMG values for each muscle were normalized to that muscle's peak value for each participant. The four left panels display normalized EMG over stride for each muscle site. The unpowered exoskeleton profiles were dashed to help differentiate them from the powered exoskeleton profiles. The right two panels show the average and peak EMG, averaged across all four muscles. * $p < 0.05$

CHAPTER 4: DISCUSSION

4.1 Hypotheses and Major Results

During the course of this study, an NMM based controller was developed and evaluated for use with a tethered exoskeleton simulator that can bilaterally generate torque about the ankles. Evaluation focused on varying gait speed and measuring metabolic rate, kinematics, kinetics, and EMG responses. I hypothesized that the exoskeleton torque and positive work rate would vary with the walking speed, replacing a portion of the biologically provided moment and decreasing metabolic energy consumption.

Average torque assistance did not successfully increase with gait speed. As gait speed increased, the MTU model demanded less torque due to a combination of the activation dynamics, kinematics, and force-length and force-velocity relationships that decreased the virtual MTU's activation. However, the exoskeleton still produced torque at all speeds and the expectation was that this torque would decrease metabolic energy consumption, even if sub-optimally. Unexpectedly, the results did not support this prediction. Metabolic energy consumption in the powered condition was not significantly changed at any walking speed compared to the metabolic energy consumption in the unpowered exoskeleton condition. Metabolic energy consumption was reduced very slightly at the lowest walking speed and was increased at the higher two walking speeds, and was higher than the no exoskeleton condition. At a walking speed of 1.25 ms^{-1} the metabolic reduction was less than 0.2%, and at the higher two speeds the metabolic increase was as much as 3.0%.

4.2 Exoskeleton Torque and Work Rate

Looking at the internal states of the NMM controller provides evidence that as speed increased, the virtual activation was significantly reduced, and this caused the reduction in virtual MTU force (**Figure 6**). The virtual activation is dependent on the activation dynamics of the muscle, which are time dependent (**Eqn. 1.5**). The less time given for activation to reach a desired activation level, the lower the level of activation obtained. Stride time decreased as walking speed increased. Because activation dynamics are time dependent and stride time was decreased, activation decreased as walking speed increased.

Additionally, kinematics, and the force-length (**Eqn. 1.8, 1.9**) and force-velocity relationships (**Eqn. 1.10, 1.11**) can affect virtual MTU force production. When the CE's contraction velocity increases, it decreases the virtual MTU potential force generation. However, there was no significant difference in CE contraction velocity across walking speeds in the powered condition (**Figure 8**).

There was significantly greater CE shortening, SEE lengthening, and MTU lengthening at the slowest walking speed compared to the fastest walking speed (**Figure 7**, **Figure 8**). CE shortening is higher at the slowest walking speed because, while CE contraction velocities are not significantly different, the stride time over which these velocities operate is longer at the slower walking speed. This causes a greater shortening of the CE at the slowest walking speed.

MTU lengthening (**Figure 7**) is higher at the slowest walking speed because the ankle sees greater dorsiflexion and less plantarflexion during walking compared to the fastest walking speed (**Figure 5**). MTU length is directly related to ankle angle (**Eqn. 1.1**).

SEE length change (**Figure 7**) is greatest at the slowest walking condition because SEE length was calculated as the difference between MTU length and CE length (**Eqn. 1.3**), and at the slowest walking speed the MTU length (**Figure 7**) is increased and the CE length (**Figure 8**) is decreased, causing a larger difference between the two. SEE length is directly related to virtual MTU force (**Eqn. 1.12**). This decrease in SEE length causes a decrease in virtual MTU force; this decreased virtual MTU is returned through the NMM feedback loop (**Figure 1**) where it causes a further decrease in activation.

4.2.1 Effect of Activation Dynamics on Activation

Simulations of the controller's internal states were performed using exoskeleton ankle angles collected during powered walking trials at each speed for each subject (**Figure 12**). The purpose of these simulations was to determine the relative contributions of activation dynamics, kinematics and force-length and force-velocity relationships to the decrease in activation as walking speed increased.

To determine the effect that activation dynamics and stride time had on activation during walking trials at 1.50 ms^{-1} and 1.75 ms^{-1}, the activation for each walking trial was simulated once normally, and then simulated a second time with the stride adjusted to match the stride time of that participant's 1.25 ms^{-1} walking trial.

The simulation results showed that at the highest walking speed, activation dynamics were responsible for causing a significant (1-sample t-test: $p = 0.012$) decrease of 20.5% in activation compared to activation obtainable at the slowest walking speed (**Figure 12**A). The activation decreases due to activation dynamics were non-significant (1-sample t-test: $p = 0.147$) at walking speeds of 1.50 ms^{-1}. 1-sample t-tests were performed to show that the there was a non-zero decrease in activation.

4.2.1 Effect of Kinematics, Force-Length, and Force-Velocity Relationships on Activation

To determine the effect which kinematics, force-length and force-velocity relationships had on activation, the activation while walking with regular activation dynamics and with significantly reduced activation and deactivation time constants (to demonstrate activation with intact activation dynamics and with activation dynamics minimized) were each simulated. The change in activation due to altered activation dynamics was calculated for each walking speed and the differences between changes in activation at 1.50 ms^{-1} or 1.75 ms^{-1} and 1.25 ms^{-1} were found. The remaining change in activation was due to a combination of kinematics, force-length and force-velocity effects.

Figure 12B shows that at a walking speed of 1.75 ms^{-1}, kinematics, force-length and force-velocity effects caused a significant (1-sample t-test: $p = 0.002$) reduction in activation of 8.3%. The activation decreases due to kinematics, and the combination of force-length and force-velocity effects were not significant (1-sample t-test: $p = 0.140$) at walking speeds of 1.50 ms^{-1}. There was a significance difference between the activation decreases due to these effects at 1.50 ms^{-1} and 1.75 ms^{-1} (t-test: $p = 0.009$).

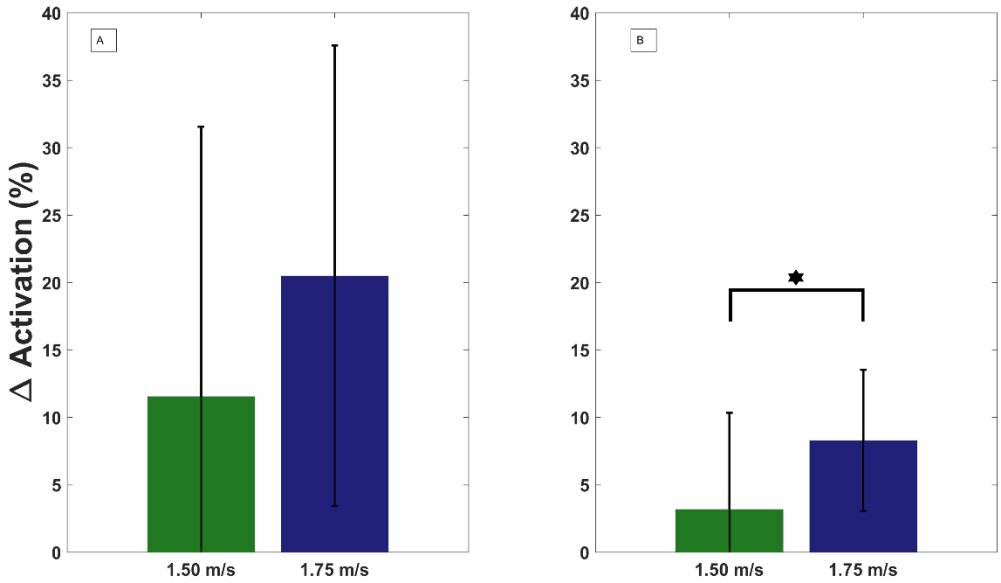

Figure 12. Simulation of Activation Decrease. The percent virtual activation decrease in the two faster powered walking conditions compared to the slowest powered walking condition due to activation dynamics (**Figure 12A**), and a combination of kinematics, force-length, and force-velocity relationships (**Figure 12B**). The decrease in virtual activation due to activation dynamics was found by using ground reaction force and ankle angle data previously recorded and using the NMM controller to simulate the activation outcome. By adjusting the stride time to match the stride time in the lowest powered walking speed it was possible to determine the decrease in activation due to activation dynamics/stride time. The role that kinematics, force-length, and force-velocity relationships had on activation was similarly determined by simulating NMM controller activation with activation dynamics minimized (to minimize its effect on activation) and determine the difference in virtual activation between the slowest walking speed and the highest walking speed. Values were averaged from all eight participants. 1-sample t-test found that the change in activation due to each set of factors was statistically significant at the fastest walking speed. * $p < 0.05$

4.3 Metabolic Energy Consumption

4.3.1 Ankle Exoskeletons Can Reduce Metabolic Energy Consumption

There is a history of successfully reducing metabolic energy consumption using ankle exoskeletons, though metabolic consumption generally sees a net increase due to the mass of the device. In some studies, exoskeletons have reduced metabolic energy consumption during walking by 24.3% [3] , 7.2% [4] ,and 6% [14]. The exoskeleton emulator, used in conjunction with the NMM controller used in the current study, has previously used non-NMM controllers to yield results where metabolic energy consumption was not significantly reduced [11], and results where metabolic energy consumption was significantly reduced [16]. This leads me to believe that the controller and not the hardware is responsible for absence of significant change in metabolic energy consumption during powered exoskeleton walking (**Figure 12**).

4.3.2 Effect of Training on Metabolic Energy Consumption

An explanation for the NMM controller's ineffectiveness at decreasing metabolic rate may be inadequate participant training with the exoskeleton. On the training day, subjects were trained in the exoskeleton for 25 minutes. Training included 5 minutes of unpowered exoskeleton walking, and 20 minutes of powered exoskeleton walking. During this training, participants were instructed to get comfortable with the exoskeleton and experiment with different gaits, but no further guidance was given. This short amount of unguided training and the short, intermittent trials during the data collection day may not have given participants adequate time to discover their optimal gait. Additionally, powered exoskeleton training was only performed at 1.25 ms^{-1}; walking in the powered condition at

higher speeds was only experienced during walking trials on the second day. When little or no guidance is provided, participants may not alter their gait to adapt to a powered exoskeleton for long periods of time (e.g., 12 minutes). When instructed to explore different gaits, it still take several minutes to metabolically optimize use of an exoskeleton [28]. Expertise and practice may be even more important at higher walking speeds, and participants may have been unable to take proper advantage of the exoskeletons during the higher speed trials. This may explain the controller's poor performance in metabolic rate reduction at higher speeds. Guiding the participant through different gaits and stride lengths at each speed may have allowed optimal conditions to be identified and a more structured training may have led to greater expertise on the participants' part.

4.3.3 Discomfort During Powered Exoskeleton Walking

During some trials, participants expressed feeling discomfort, particularly fatigue in the TA muscle. In some instances, the participant needed to reschedule the data collection, and in one case chose not to continue with the study. Pain or discomfort can alter kinematics during walking [29] and affect athletic performance [30]. This discomfort may have caused subjects to alter their gait, shifting the focus from metabolically efficient walking to pain avoidance. Discomfort in the TA during powered exoskeleton walking may have been due to increased TA activation in the powered walking condition (**Figure 11**).

4.3.4 Asymmetric Torque Application

Exoskeletons were worn on both legs and were used to apply bilateral torque, but the application of torque was observed to not always be symmetric. Sometimes the

subject's dominant foot would receive up to 20% more torque than the non-dominant foot, though exact quantitative comparisons cannot be made because only right leg exoskeleton torque data was saved. This difference in torque application was not consistent, appeared intermittently, and seemed to be related to foot dominance, rather than either the left or right foot. This may have increased metabolic energy consumption by making the gait asymmetric, which is known to increase metabolic energy consumption [31], [32].

4.3.5 Exoskeleton Torque Profile

It was expected that the NMM controller would produce significant reductions in metabolic energy consumption by mimicking biological muscle torque profiles, but results did not support this expectation. In fact, Malcolm et al. [14] found that non-biologically inspired actuation onset timing of an ankle exoskeleton caused the greatest reduction in metabolic energy consumption when actuation was initiated at 43% of the stride cycle, instead of the biologically typical 15%. When actuation was applied later in the stride cycle, they could achieve a metabolic reduction several times greater. The NMM controller in the current study was intended to mimic biological actuation and it applied torque around 5% of the stride (**Figure 3**), which is even earlier than the biologically typical point. Additionally, Malcolm reported that their exoskeleton produced no significant negative work due to the late actuation onset, whereas my NMM controller produced significant negative work early in the stride cycle (**Figure 3**).

Sawicki et al. [4] used a passive ankle exoskeleton to reduce metabolic energy consumption during walking by up to 7.2 ± 2.6%, and found that with increased stiffness of

the exoskeleton spring the metabolic rate would increase. Their exoskeleton began generating torque around 10% of stride and peaked around 50% stride, similar to the torque profile produced by the NMM controller used in the current study (**Figure 3**). However, they produced much lower amounts of torque and investigated slower walking speeds, which may partially account for the differences in metabolic outcomes.

4.3.6 Work versus Torque for Reductions in Metabolic Energy Consumption

Jackson and Collins [13] varied work and torque assistance in ankle exoskeletons over a large range. A focus on producing a large amount of work caused a large amount of torque late in the stride cycle (35-60%). A focus on high torque production caused torque onset around 5% of the stride cycle and reduced torque after 40% stride. They found that increasing work can decrease metabolic consumption and increasing torque can increase metabolic consumption. However, they noted that effects on the metabolic rate were due to whole body coordination, which may have been influenced by the fact that they were unilaterally applying torque.

One study compared the impacts of a unilateral ankle exoskeleton at 1.25 ms^{-1} walking speed with the exoskeleton performing work during plantarflexion versus providing high torque (and no work) earlier in stance phase [1]. Interestingly, this study found that when the exoskeleton provided work they were able to decrease metabolic expenditure by 17%, but that metabolic expenditure was increased when high torque was provided. Our NMM controller provided higher torque and performed less positive work while operating

at higher speeds and had poorer metabolic outcomes, which is consistent with the results from Jackson and Collins.

4.4 Decreased Biological Ankle Torque, Maintained or Increased Metabolic Energy Consumption

Biological ankle torque (**Figure 4**) was decreased in the powered condition but metabolic energy consumption (**Figure 10**) was not reduced. Decreased biological torque found in powered exoskeleton sessions in this study may have been in part due to increased TA co-activation rather than decreased plantarflexor activation. This may have resulted in increased metabolic energy consumption rather than decreased (**Figure 11**). This increase in TA activation might be avoided in several ways. If the increase in activation is due to unfamiliarity with the exoskeleton then additional training might cause the user to decrease unnecessary activation over time. If the activation increase is due to high activation being required to achieve toe clearance during swing, then reducing exoskeleton weight and reducing exoskeleton torque when the foot is highly plantarflexed in late stance might ameliorate the problem. If high TA activation is due to torque applied by the exoskeleton during swing (**Figure 3**), then activation might be reduced by having the motor introduce slack into the Bowden cable upon the initiation of swing phase.

4.5 Potential NMM Controller Applications

This neuromuscular model-based controller may still be advantageous in some conditions where speed-dependent decreases in exoskeleton torque production would not necessarily appear, such as across different ground slopes or under loaded conditions. Also, the NMM controller might operate better at slower speeds than tested. Slower walking

speeds may increase stride times and thus avoid the decrease in virtual activation due to activation dynamics, high plantarflexion at high walking speed, and force-length and force-velocity effects in the controller (**Figure 12**), though this limits the controller's useful range.

4.5.1 Walking Under a Load

Griffen et al. looked at the metabolic energy consumption of load carrying at different walking speeds [33]. They found that while walking under a load at speeds of 1.0 ms^{-1} and faster, metabolic energy consumption was directly related to the active muscle volume and muscular force. The ability of the NMM model to decrease biologically generated force (**Figure 4**) and decrease activation of the MG (**Figure 11**) means that it may be more effective at reducing metabolic expenditure while walking under load than it was during unloaded walking.

4.5.2 NMM Control of the Hip or Knee

Wu et al. examined the use of a NMM-controlled hip and knee exoskeleton for patients with SCI [8]. This study included bilateral exoskeleton application and involved slow walking speeds. They found that the controller was able to modulate torque at different speeds, and kinematics were not significantly impacted, but they did not investigate metabolic effects. It is possible that the hip and knee are better targets for NMM control; however, this study was performed with SCI patients, with body weight support, with different controller parameters and primarily at speeds of less than 1.0 ms^{-1}, any of which may also have affected controller performance.

4.5.3 Lower Walking Speeds

The NMM Controller used here might be more successful at modulating torque with walking speed and decreasing metabolic energy consumption if operated at lower walking speeds. NMM walking simulations have achieved successful walking at relatively low walking speeds of 0.40-0.90 ms^{-1} and 0.75-1.35 ms^{-1} [9], [10] compared to the higher walking speeds of 1.25-1.75 ms^{-1} (**Figure 2**) used in the current NMM study. One study looked at the performance of a NMM controller with bilateral exoskeletons at two walking speeds [7]. They found modest decreases in metabolic expenditure at relatively low walking speed (0.58-1.08 ms^{-1}), and the controller was able to successfully decrease biological torque and work rate. Exoskeleton torque decreased at higher speeds. These findings are consistent with those of the current study.

4.5.4 Unilateral Exoskeleton Application

Previous studies [5], [6] have reported a unilateral NMM controller ankle prosthesis modulating torque over a range of walking speeds. It possible that a NMM controller may be more effective when used unilaterally, because the user may be better able to adjust to more favorable kinematics.

4.4.5 Unloading the Plantarflexor Muscles and Ankles

While the exoskeleton did not decrease overall metabolic demand, it did decrease force requirements of the soleus and gastrocnemius muscles (reduced biological torque) (**Figure 4**) and activation requirements of the MG (**Figure 11**). This could be useful for patient populations recovering from ankle injury or disuse, or who place unusually high

torque demands on the ankle. Obese adults have increased torque and power requirements at the ankle compared healthy weight adults [34]. NMM-controlled ankle exoskeletons could reduce plantarflexor fatigue, encourage socialization and exercise. Alternatively, those who are recovering from ankle injury or surgery may benefit from reduced musculoskeletal loading while preserving push-off using NMM-controlled ankle exoskeletons.

Decreased biological ankle push-off is shown to increase hip torque during walking [35]. This is consistent with our results in **Figure 14** that shows an increase in hip torque in the powered walking condition. The biological ankle torque and work rate in the exoskeleton-powered condition is decreased compared to ankle torque and work rate in the non-powered condition (**Figure 4**).

4.4.6 Plantarflexor Augmentation During Fatigued Conditions

The controller was able to reduce gastrocnemius activation (**Figure 11**) and might be able to extend the period of time a user can walk by augmenting torque produced by fatigued plantarflexor muscles. One study found that fatigued ankle flexor muscles produce reduced torque and have decreased plantarflexion [36]. Though they contend that this fatigue did not significantly impact gait mechanics, it is possible that greater fatigue, bilateral fatigue or loaded conditions would have caused greater impact to become apparent. A NMM-controlled ankle exoskeleton may be able to compensate for fatigued plantarflexor muscles in these cases.

4.5 Potential NMM Controller Improvements

While the NMM controller did not perform successfully in the range of walking speeds tested, it is possible that the controller might perform better by incorporating a feedforward component, adjusting parameters with walking speed, or by modeling the soleus and gastrocnemius as separate muscles instead of as a combined plantarflexor muscle.

4.5.1 Incorporating a Feedforward Component into the NNM Controller

The NMM controller used had reflex-based feedback but had no feedforward component (**Figure 1**). The lack of a feedforward component may be responsible for the decrease in activation seen at higher walking speeds. NMM walking simulations have successfully reached relatively high walking speeds when incorporating a feedforward component [9], [10]. Proportional myoelectric propulsion, which uses EMG as a feedforward controller component, is able to increase exoskeleton torque with walking speed [11].

One study was able to successfully simulate a bipedal walker using a neuromuscular model and modulate its walking speed over a range of 0.4 – 0.9 ms^{-1} [9]. This simulation was performed at slower walking speeds which may have improved performance of the controller, indicating that NMM control is appropriate for slower speeds. Additionally, they incorporated both reflex based feedback and feedforward (CPG) components which may have improved performance at the higher speeds simulated. Another study modeled a

NMM controller with CPG feedforward components and were able to successfully modulate speed between 0.75-1.35 ms^{-1} [10].

One study used a proportional myoelectric propulsion controller to control a unilateral ankle exoskeleton to improve post-stroke gait [11]. The proportional myoelectric propulsion controlled exoskeleton was able to slightly decrease metabolic expenditure, and was able to increase ankle torque but not positive work at the ankle.

Combining a feedforward component, such as proportional myoelectric propulsion, with a feedback based NMM controller may allow for a controller that performs positive work about the ankle and is able to maintain increases in work rate and ankle torque at higher walking speeds.

4.5.2 Adjusting Controller parameters with Walking Speed

Many of the NMM controller's parameters were invariant with walking speed, and were optimized specifically for walking speeds well below the walking speed range the on which the controller was tested.

A feedback gain of 1.2 was applied in our NMM controller according to a value reported in Eilenberg et al. 2009 [5]. This feedback gain value was optimized to match a neuromuscular model's torque profiles to biological torque 1 ms^{-1} walking speed, instead of optimizing the parameter for multiple walking speeds. One study found that various feedback gains are adjusted to the task during task performance, including the force feedback gain [37]. Adjustment of the force feedback gain can be used to alter hopping task outcomes [21]. By optimizing this feedback gain for different walking speeds and adjusting

the gain according to walking, it may be possible to improve the NMM controller's performance and ability to increase exoskeleton torque with walking speed.

4.5.3 Multiple Joint Inputs into NMM Controller

The NMM controller only used the ankle angle as an input (**Figure 1**). However, the length and strain of the SOL, MG and LG muscles are also affected by the knee joint angle [38]. Knee and hip joint angles during powered exoskeleton walking diverged some from the angle profile of unpowered exoskeleton walking, especially as walking speed increased (**Figure 13**). By measuring the ankle and knee joint angles and incorporating both into the NMM model, it may be possible to improve controller performance.

4.5.4 Modeling the Soleus and Gastrocnemius Separately

The virtual MTU used in the NMM controller was modeled as a single plantarflexor muscle based on a combination of characteristics of the soleus and gastrocnemius muscles. Previous work with NMM prosthesis control used similar MTU models which combined multiple plantarflexor muscles into a single model [5], [6]. This may be more computationally efficient than modeling multiple muscles but modeling individual muscles may allow for improved controller operation across a wider range of conditions. For example, the NMM controller used activation dynamics constants of τ_{act} = 33 ms, and τ_{dact} =91 ms, and these constants played a significant role in the decrease of exoskeleton torque at high walking speeds (**Figure 12**). The gastrocnemius has more rapid activation dynamics than used in the NMM controller (τ_{act} = 25 ms, τ_{dact} = 42 ms) [39]. By modeling the gastrocnemius separately from the soleus, the controller might be able to take advantage of

these faster activation dynamics and improve high walking speed performance. Additionally, one study found that the SOL, MG and LG behaved similarly under high force, low speed cycling conditions, and less similarly at higher speed cycling conditions [39]. This indicates that the controller benefits of separately modeling the SOL, MG, and LG might be most evident at higher walking speeds. Additionally, it has been found that recruitment of fast motor units increases with more rapid locomotion [40]. Incorporating these relationships into the controller would allow for an increase in virtual gastrocnemius activation at high walking speeds. An NMM simulation (similar to that described in **Figure *12***), with the activation dynamics changed to match those of the gastrocnemius, was performed using data from all eight participants walking at 1.75 ms^{-1} in the powered exoskeleton condition. It was found that this change in activation dynamics caused a 5.80% ± 1.35 increase in activation.

CHAPTER 5: CONCLUSIONS

For this study, a neuromuscular model-based controller was developed for use with a tethered exoskeleton simulator that can bilaterally generate torque about the ankles. The controller and exoskeleton combination was evaluated for its effect on gait over level terrain at a set gain based on calculated biological moment. Gait speed was tested over a significant range. Outcomes for characterizing participant response to the exoskeleton and controller at different speeds included metabolic rate, kinematics, kinetics, and EMG. It was hypothesized that the exoskeleton would generate torque, and work, and reductions of metabolic energy consumption, and each of these would increase as walking speed increased from 1.25 to 1.75 ms^{-1}.

There was no significant change in metabolic energy consumption at any speed in the powered exoskeleton condition compared to the unpowered exoskeleton condition. There was, however, a reduction in biologically produced negative work in the powered walking condition compared to the unpowered walking condition. The results suggest that a reduction in biological work may have been due to increased TA co-activation and not just due to reduced plantarflexor activation, which is why metabolic energy consumption increased or was unchanged. Increased TA activation in the powered condition may have also caused plantarflexor activation to be higher than it otherwise would have been, thus further increasing metabolic energy consumption. As speed increased the controller instructed the exoskeleton to produce less torque due to shorter stride times, thereby causing the virtual CE to become less fully activated due to activation dynamics, as well as kinematic and force-length and force-velocity interactions. This reduced MTU force, which

further reduced activation. Exoskeleton positive and negative work rate were maintained or increased across walking speeds due to more frequent strides at higher walking speeds.

Future controllers could incorporate proportional myoelectric components into the NMM controller. Using EMG signals as feedforward elements might allow for the controller to account for increased biological muscle activation, which could counteract the decreased virtual activation. Improved training and adjusting controller gain with walking speed could also lead to better results using an NMM controller.

REFERENCES

[1] R. W. Jackson and S. H. Collins, "An experimental comparison of the relative benefits of work and torque assistance in ankle exoskeletons," *J. Appl. Physiol.*, vol. 119, no. 5, pp. 541–557, 2015.

[2] M. R. Tucker *et al.*, "Control Strategies for Active Lower Extremity Prosthetics and Orthotics : A Review," *J. Neuroeng. Rehabil.*, vol. 12, no. 1, 2015.

[3] J. Zhang *et al.*, "Human-in-the-loop optimization of exoskeleton assistance during walking," *Science (80-.).*, vol. 356, no. 6344, pp. 1280–1284, 2017.

[4] S. H. Collins, M. B. Wiggin, and G. S. Sawicki, "Reducing the energy cost of human walking using an unpowered exoskeleton," *Nature*, vol. 522, no. 7555, pp. 212–215, 2015.

[5] Eilenberg, M.F., Geyer, H., and Herr, H., "Control of a Powered Ankle–Foot Prosthesis Based on a Neuromuscular Model," *IEEE Trans. Neural Syst. Rehabil. Eng.*, vol. 18, no. 2, pp. 164–173, 2010.

[6] J. Markowitz, P. Krishnaswamy, M. F. Eilenberg, K. Endo, C. B. Chris, and H. Herr, "Speed adaptation in a powered transtibial prosthesis controlled with a neuromuscular model," *Philos. Trans. R. Soc. B Biol. Sci.*, vol. 366, no. 1570, pp. 1621–1631, 2011.

[7] F. Dzeladini *et al.*, "Effects of a neuromuscular controller on a powered ankle exoskeleton during human walking," *2016 6th IEEE Int. Conf. Biomed. Robot. Biomechatronics*, pp. 617–622, 2016.

[8] A. R. Wu, F. Dzeladini, T. J. H. Brug, and F. Tamburella, "An Adaptive Neuromuscular Controller for Assistive Lower-Limb Exoskeletons : A Preliminary Study on Subjects with Spinal Cord Injury," *Front. Neurorobot.*, vol. 11, pp. 1–14, 2017.

[9] N. Van der Noot, A. J. Ijspeert, and R. Ronsse, "Neuromuscular model achieving speed control and steering with a 3D bipedal walker," *Auton. Robots*, vol. 43, no. 6, pp. 1537–1554, 2018.

[10] F. Dzeladini, J. van den Kieboom, and A. Ijspeert, "The contribution of a central pattern generator in a reflex-based neuromuscular model," *Front. Hum. Neurosci.*, vol. 8, pp. 1–18, 2014.

[11] E. M. McCain *et al.*, "Mechanics and energetics of post-stroke walking aided by a powered ankle exoskeleton with speed-adaptive myoelectric control," *J. Neuroeng. Rehabil.*, vol. 16, no. 1, 2019.

[12] D. J. Farris and G. S. Sawicki, "The mechanics and energetics of human walking and running: a joint level perspective.," *J. R. Soc. Interface*, vol. 9, no. 66, pp. 110–118, 2012.

[13] R. W. Jackson and S. H. Collins, “An experimental comparison of the relative benefits of work and torque assistance in ankle exoskeletons,” *J. Appl. Physiol.*, vol. 119, no. 5, pp. 541–557, 2015.

[14] P. Malcolm, W. Derave, S. Galle, and D. De Clercq, “A Simple Exoskeleton That Assists Plantarflexion Can Reduce the Metabolic Cost of Human Walking,” *PLoS One*, vol. 8, no. 2, pp. 1–7, 2013.

[15] A. C. De David, F. P. Carpes, and D. Stefanyshyn, “Effects of changing speed on knee and ankle joint load during walking and running,” *J. Sports Sci.*, vol. 33, no. 4, pp. 391–397, 2015.

[16] R. W. Nuckols, “Effects of Elastic Ankle Exoskeleton Stiffness and Walking Speed on Human Locomotor Performance from Whole-Body Energetics to Individual Muscle Neuromechanics,” North Carolina State University, 2017.

[17] A. V. Hill, “The Heat of Shortening and the Dynamic Constants of Muscle,” *Proc. R. Soc. London . Ser. B , Biol. Sci.*, vol. 126, no. 843, pp. 136–195, 1938.

[18] J. M. Winters and L. Stark, “Estimated mechanical properties of synergistic muscles involved in movements of a variety of human joints,” *J. Biomech.*, vol. 21, no. 12, pp. 1027–1041, 1988.

[19] B. D. Robertson and G. S. Sawicki, “Exploiting elasticity : Modeling the influence of neural control on mechanics and energetics of ankle muscle – tendons during human hopping,” *J. Theor. Biol.*, vol. 353, pp. 121–132, 2014.

[20] C. C. Raasch, F. E. Zajac, B. Ma, and W. S. Levine, “Muscle coordination of movement of maximum-speed pedaling,” *J. Biomech.*, vol. 30, no. 6, pp. 595–602, 1993.

[21] H. Geyer, A. Seyfarth, and R. Blickhan, “Positive force feedback in bouncing gaits?,” *Proc. Biol. Sci.*, vol. 270, no. 1529, pp. 2173–83, 2003.

[22] A. L. Hof, J. P. Van Zandwijk, and M. F. Bobbert, “Mechanics of human triceps surae muscle in walking, running and jumping,” *Acta Physiol. Scand.*, vol. 174, no. 1, pp. 17–30, 2002.

[23] E. Azizi and T. J. Roberts, “Muscle performance during frog jumping: Influence of elasticity on muscle operating lengths,” *Proc. R. Soc. B Biol. Sci.*, vol. 277, no. 1687, pp. 1523–1530, 2010.

[24] E. Otten, “A myocybernetic model of the jaw system of the rat,” *J. Neurosci. Methods*, vol. 21, no. 2–4, pp. 287–302, 1987.

[25] G. S. Sawicki and N. S. Khan, “A simple model to estimate plantarflexor muscle - tendon mechanics and energetics during walking with elastic ankle exoskeletons,” *IEEE Trans. Biomed. Eng.*, vol. 63, no. 5, pp. 914–923, 2015.

[26] K. Z. Takahashi, M. D. Lewek, and G. S. Sawicki, “A neuromechanics-based powered ankle exoskeleton to assist walking post-stroke: a feasibility study,” *J. Neuroeng.*

Rehabil., vol. 12, no. 1, p. 23, 2015.

[27] J. M. Brockway, “Derivation of formulae used to calculate energy expenditure in man,” *Hum. Nutr. Clin. Nutr.*, vol. 41, no. 6, pp. 463–471, 1987.

[28] J. C. Selinger, S. M. O’Connor, J. D. Wong, and J. M. Donelan, “Humans Can Continuously Optimize Energetic Cost during Walking,” *Curr. Biol.*, vol. 25, no. 18, pp. 2452–2456, 2015.

[29] R. S. Macphee, K. McFall, S. D. Perry, and P. M. Tiidus, “Metabolic cost and mechanics of walking in women with fibromyalgia syndrome,” *BMC Res. Notes*, vol. 6, no. 1, 2013.

[30] M. Kinchington, K. Ball, and G. Naughton, “Relation between lower limb comfort and performance in elite footballers,” *Phys. Ther. Sport*, vol. 13, no. 1, pp. 27–34, 2012.

[31] C. Detrembleur, F. Dierick, G. Stoquart, F. Chantraine, and T. Lejeune, “Energy cost, mechanical work, and efficiency of hemiparetic walking,” *Gait Posture*, vol. 18, no. 2, pp. 47–55, 2003.

[32] C. J. Wutzke, G. S. Sawicki, and M. D. Lewek, “The influence of a unilateral fixed ankle on metabolic and mechanical demands during walking in unimpaired young adults,” *J. Biomech.*, vol. 45, no. 14, pp. 2405–2410, 2012.

[33] T. M. Griffin, T. J. Roberts, and R. Kram, “Metabolic cost of generating muscular force in human walking: insights from load-carrying and speed experiments,” *J. Appl. Physiol.*, vol. 95, no. 1, pp. 172–183, 2015.

[34] P. DeVita and T. Hortobágyi, “Obesity is not associated with increased knee joint torque and power during level walking,” *J. Biomech.*, vol. 36, no. 9, pp. 1355–1362, 2003.

[35] C. L. Lewis and D. P. Ferris, “Walking with increased ankle pushoff decreases hip muscle moments.,” *J. Biomech.*, vol. 41, no. 10, pp. 2082–9, 2008.

[36] M. A. Hunt and G. L. Hatfield, “Ankle and knee biomechanics during normal walking following ankle plantarflexor fatigue,” *J. Electromyogr. Kinesiol.*, vol. 35, pp. 24–29, 2017.

[37] W. Mugge, D. A. Abbink, A. C. Schouten, J. P. A. Dewald, and F. C. T. Van Der Helm, “A rigorous model of reflex function indicates that position and force feedback are flexibly tuned to position and force tasks,” *Exp. Brain Res.*, vol. 200, pp. 325–340, 2010.

[38] P. A. Huijing, A. Yaman, C. Ozturk, and C. A. Yucesoy, “Effects of knee joint angle on global and local strains within human triceps surae muscle: MRI analysis indicating in vivo myofascial force transmission between synergistic muscles,” *Surg. Radiol. Anat.*, vol. 33, no. 10, pp. 869–879, 2011.

[39] T. J. M. Dick, A. A. Biewener, and J. M. Wakeling, “Comparison of human

gastrocnemius forces predicted by Hill-type muscle models and estimated from ultrasound images," *J. Exp. Biol.*, vol. 220, no. 9, pp. 1643–1653, 2017.

[40] S. S. M. Lee, M. De Boef Miara, A. S. Arnold, A. A. Biewener, and J. M. Wakeling, "Recruitment of faster motor units is associated with greater rates of fascicle strain and rapid changes in muscle force during locomotion," *J. Exp. Biol.*, vol. 216, no. 2, pp. 198–207, 2013.

APPENDIX

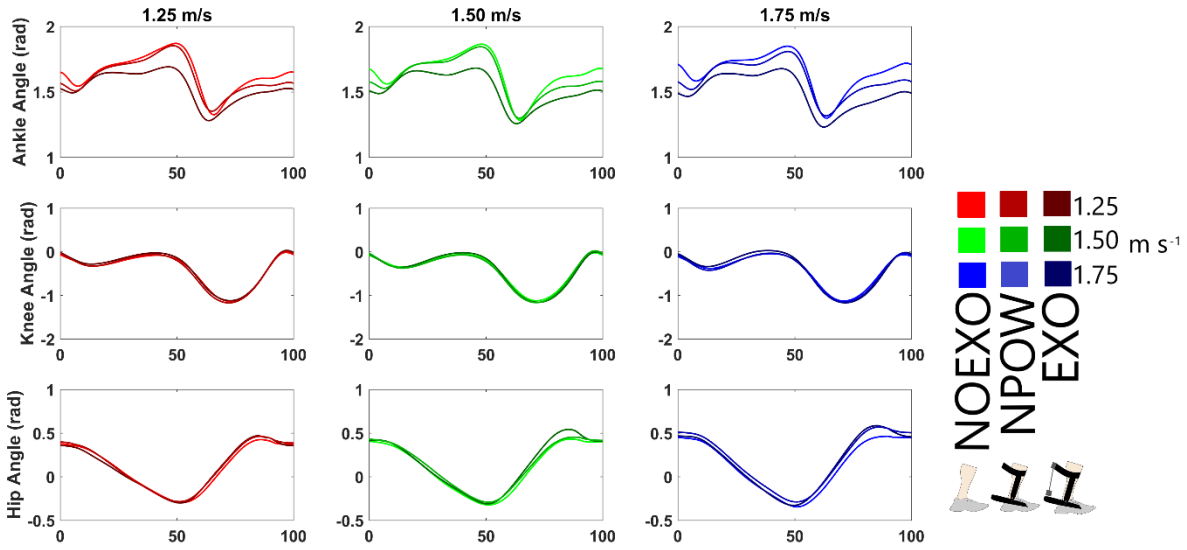

Figure 13. Lower-limb Joint Kinematics. Joint angle of ankle, knee and hip. The lightest colored lines represents no exoskeleton data, and the darkest lines represent unpowered and powered exoskeleton data.

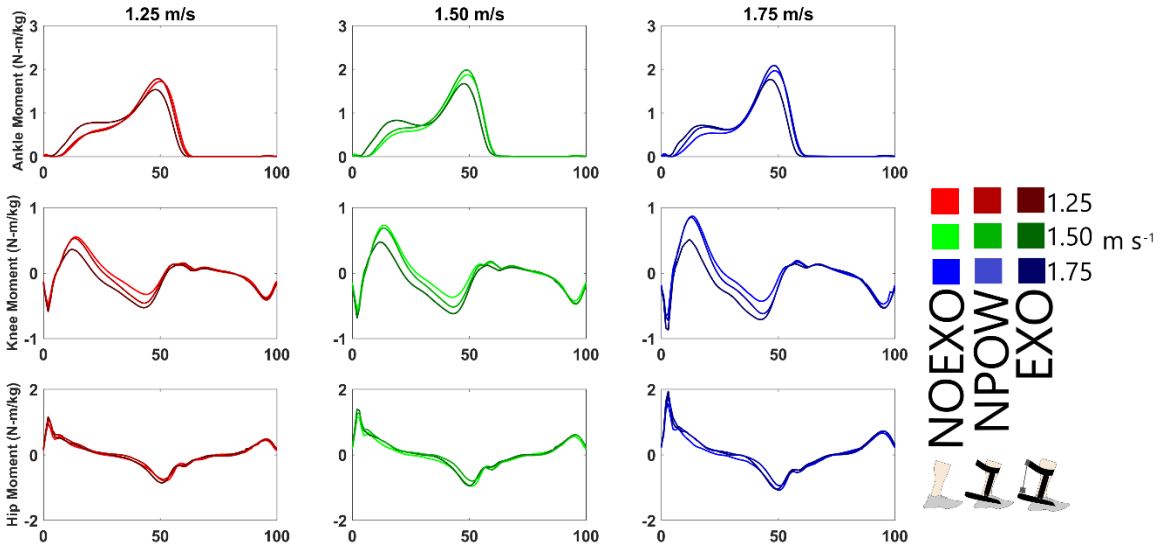

Figure 14. Lower-limb Joint Moment. Joint torque of ankle, knee and hip. The lightest colored lines represents no exoskeleton data, and the darkest lines represent unpowered and powered exoskeleton data.

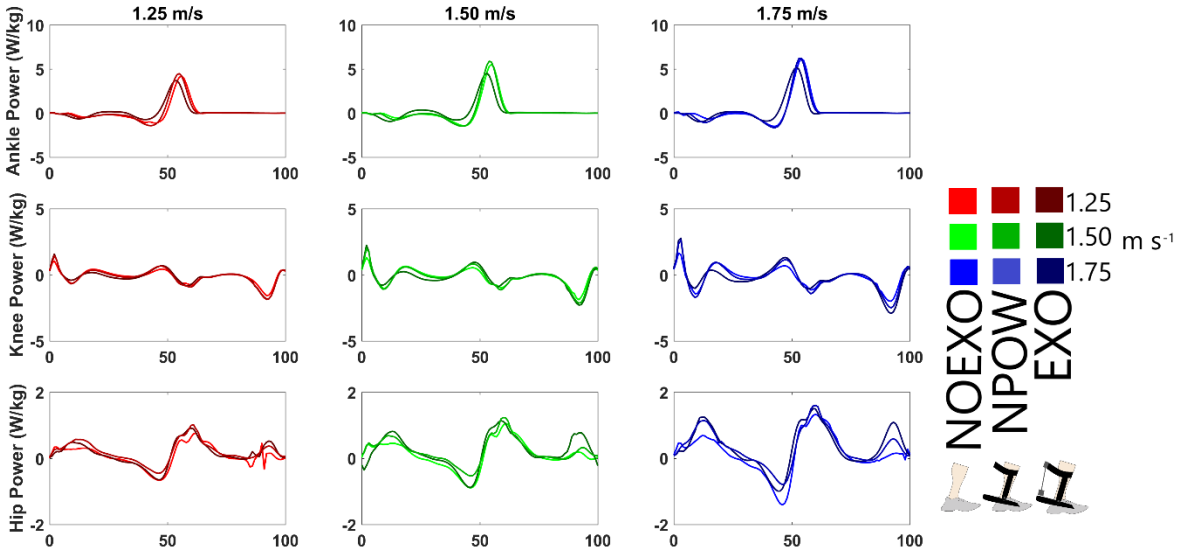

Figure 15. Lower-limb Joint Power. Joint power of ankle, knee and hip. The lightest colored lines represents no exoskeleton data, and the darkest lines represent unpowered and powered exoskeleton data.